Article

A Novel Three-Vector-Based Model Predictive Direct Power Control for Three-Phase PWM Rectifier

Liuchen Tai [1],*, Mingyao Lin [2], Hui Li [3] and Yongsheng Li [4]

1 College of Information and Control Engineering, Weifang University, Weifang 261061, China
2 School of Electrical Engineering, Southeast University, Nanjing 210096, China; mylin@seu.edu.cn
3 Electric Power Research Institute of Guangdong Power Grid Ltd., Guangzhou 510080, China; lihuiseu@163.com
4 Shandong Tianrui Heavy Industry Co., Ltd., Weifang 261061, China; tr9909@126.com
* Correspondence: tailiuchen@163.com; Tel.: +86-133-7105-5879

Abstract: A novel strategy of three-vector-based model predictive direct power control (MPDPC) is proposed for three-phase Pulse-width Modulation (PWM) rectifier. Under ideal grid conditions, three-vector MPDPC is studied, and a good control effect has been achieved. However, under the unbalanced power grid condition, the traditional control strategy has some problems, such as a high harmonic content of current and large instantaneous power pulsation. A new three-vector model predictive control is proposed based on the new instantaneous power theory, and the objective function is established by instantaneous power error. The duty cycle of the selected vector is calculated by solving the optimal objective function. Under an unbalanced power grid, this paper takes a three-phase PWM rectifier as a research object, and carries out simulation and experimental tests on the traditional and new control strategies. The experimental results show that the new control strategy has lower current harmonics, and eliminates the twice grid-frequency oscillation of the grid in instantaneous power.

Keywords: three-phase PWM rectifier; three-vector; model predictive direct power control; new instantaneous power theory; unbalanced grid conditions

1. Introduction

In the discrete mathematical model of PWM rectifier, the model predictive control (MPC) predicts the grid side current, instantaneous power and other electrical quantities in the next control cycle; then the objective function is set according to the needs of the control system, an optimal voltage vector is obtained by solving the optimal objective function [1–6]. As a kind of predictive control, it has the advantages of not having a pulse width modulation module, flexible control scheme and high robust performance, and as such has aroused the interest of many scholars [7–12].

The finite control set model predictive direct power control (FCS-MPDPC) combines MPC with DPC [13–15]. The objective function of FCS-MPDPC is composed of the error term between the instantaneous power and the given value, and an appropriate voltage vector is selected by solving the optimal objective function, which improves the control performance of the rectifier while maintaining a fast dynamic response. However, this method uses one voltage vector in a switching cycle. To achieve better control performance, the sampling frequency of the control system must be increased. Reference [6] proposed a FCS-MPDPC, based on duty cycle optimization, which is also known as two-vector FCS-MPDPC. Different from the traditional FCS-MPDPC, the control method uses a zero vector and a non-zero vector in one cycle, and uses the zero-vector to regulate the instantaneous power smoothly. The two-vector FCS-MPDPC can maintain a fast dynamic response under the same sampling frequency, and at the same time reduce the current harmonic content and reduce the instantaneous power pulsation. Reference [16] also proposes a

two-vector FCS-MPDPC. The main difference between reference [16] and reference [6] is that reference [6] takes the minimum sum of squares of instantaneous power error as the optimization objective, while reference [16] takes the minimum instantaneous active power ripple as the control objective. These two strategies can achieve good control effect, but there is a certain coupling relationship in the control of instantaneous power. That is, when the instantaneous active power changes suddenly, it will affect the control of instantaneous reactive power, and even cause a fluctuation of instantaneous reactive power, and vice versa.

To solve this problem, a power decoupled FCS-MPDPC is proposed in reference [17]. In this algorithm, weight coefficients are introduced into the instantaneous power error terms, and the weight coefficients will change with the changes in instantaneous power errors. The two-vector in references [6], [16] and [17] are composed of the zero-vector. Based on the principle of volt second balance, the two-vector cannot synthesize the voltage vector of any angle in the plane, so they cannot fully meet the requirements of grid-connected control of PWM rectifier. Therefore, a new type of FCS-MPDPC is proposed in reference [18], that is, a non-zero-vector can be combined not only with zero-vector, but also with adjacent non-zero vectors. There are 12 different vector combinations. Through the expansion of a vector combination, the algorithm can reduce the instantaneous power ripple and the harmonic content of current to a certain extent, but it cannot achieve a fixed switching frequency. In reference [19], a three-vector FCS-MPDPC is proposed, which uses two non-zero vectors and one zero-vector. This algorithm has the advantages of high sinusoidal current, small instantaneous power ripple and the switching frequency is fixed. In reference [20], a three-vector FCS-MPDPC is proposed to optimize the switching sequence. Different from reference [19], the algorithm needs to predict the instantaneous power under 12 different vector combinations, and sets an objective function, based on the global power error, that is, to accumulate the sum of squares of the instantaneous power error terms in each switching action in a control cycle. Although the algorithm can further suppress the power ripple, reduce the total harmonic distortion (THD) and obtain a fixed switching frequency, it needs to predict the instantaneous power twelve times, which is complex and requires high processing speed of the control chip.

In addition, under three-phase unbalanced power grid condition, the negative sequence component will appear in the grid voltage. If the traditional FCS-MPDPC is still used, the THD of the grid side current will be larger and the instantaneous power ripple will be larger. Therefore, based on the new instantaneous power theory, a new three-vector FCS-MPDPC is proposed.

2. Mathematical Model of PWM Rectifier

Figure 1 is the three-phase PWM rectifier. Among them, e_a, e_b and e_c are three-phase grid voltage, i_a, i_b and i_c are three-phase grid current, v_a, v_b and v_c are three-phase bridge arm output voltage of PWM rectifier. L is inductance. R is parasitic resistance.
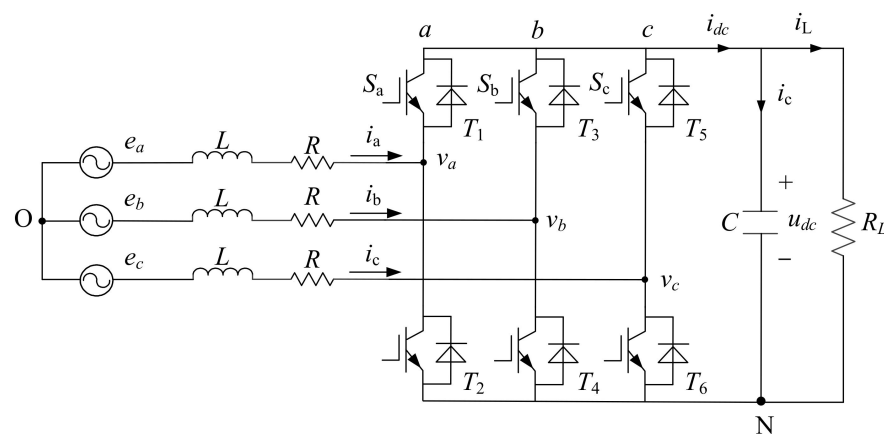

Figure 1. Three-phase PWM rectifier.

Based on Kirchhoff voltage law, the voltage loop equation of AC side of PWM rectifier is:

$$\begin{cases} L\frac{di_a}{dt} + Ri_a = e_a - v_a \\ L\frac{di_b}{dt} + Ri_b = e_b - v_b \\ L\frac{di_c}{dt} + Ri_c = e_c - v_c \end{cases} \tag{1}$$

The corresponding vector equation is:

$$\boldsymbol{E} = L\frac{d\boldsymbol{I}}{dt} + R\boldsymbol{I} + \boldsymbol{V} \tag{2}$$

where, $\boldsymbol{E}$ means the three-phase grid voltage vector. $\boldsymbol{I}$ means the three-phase grid current vector. $\boldsymbol{V}$ means the AC side output voltage vector of PWM rectifier.

Through abc/$\alpha\beta$ coordinate transformation, the PWM rectifier in the $\alpha\beta$ coordinate system is:

$$\begin{cases} L\frac{di_\alpha}{dt} = e_\alpha - Ri_\alpha - v_\alpha \\ L\frac{di_\beta}{dt} = e_\beta - Ri_\beta - v_\beta \end{cases} \tag{3}$$

where, e_α and e_β are components of $\boldsymbol{E}$, i_α and i_β are components of $\boldsymbol{I}$, and v_α and v_β are components of $\boldsymbol{V}$.

When the three-phase grid is unbalanced, the fundamental component is considered, in dq coordinate system the $\boldsymbol{E}$ is:

$$\boldsymbol{E} = e^{j\omega t}E_{dq}^P + e^{-j\omega t}E_{dq}^N \tag{4}$$

where, E_{dq}^P and E_{dq}^N are the fundamental voltage component of positive sequence and negative sequence.

Assuming that both $\boldsymbol{V}$ and $\boldsymbol{I}$ have positive and negative sequence components, we can get the following conclusion:

$$\begin{cases} \boldsymbol{V} = e^{j\omega t}V_{dq}^P + e^{-j\omega t}V_{dq}^N \\ \boldsymbol{I} = e^{j\omega t}I_{dq}^P + e^{-j\omega t}I_{dq}^N \end{cases} \tag{5}$$

where, V_{dq}^P and V_{dq}^N are positive sequence and negative sequence fundamental voltage components, respectively, I_{dq}^P and I_{dq}^N are positive sequence and negative sequence fundamental current components, respectively.

2.1. Traditional Instantaneous Power in dq Coordinate System

Based on the instantaneous power theory [21], the complex power $\boldsymbol{S}$ is:

$$\boldsymbol{S} = 1.5\boldsymbol{I}^*\boldsymbol{E} = 1.5\left(e^{j\omega t}I_{dq}^P + e^{-j\omega t}I_{dq}^N\right)^*\left(e^{j\omega t}E_{dq}^P + e^{-j\omega t}E_{dq}^N\right) \tag{6}$$

where, "*" denotes the conjugation of related variables. The instantaneous active and reactive power expressions is:

$$\begin{cases} p = 1.5\text{Re}(\boldsymbol{I}^*\boldsymbol{E}) = p_0 + p_{c2}\cos(2\omega t) + p_{s2}\sin(2\omega t) \\ q = 1.5\text{Im}(\boldsymbol{I}^*\boldsymbol{E}) = q_0 + q_{c2}\cos(2\omega t) + q_{s2}\sin(2\omega t) \end{cases} \tag{7}$$

where, p_0 and q_0 are the DC components of instantaneous power, p_{c2} and q_{c2} are cosine components peak of the second order of instantaneous power, p_{s2} and q_{s2} are sine components peak of the second order of instantaneous power.

Further, the peak value of each component can be deduced as follows:

$$
\begin{cases}
p_0 = 1.5(E_{dq}^P \odot I_{dq}^P + E_{dq}^N \odot I_{dq}^N) = 1.5(e_d^P i_d^P + e_q^P i_q^P + e_d^N i_d^N + e_q^N i_q^N) \\
p_{c2} = 1.5(E_{dq}^N \odot I_{dq}^P + E_{dq}^P \odot I_{dq}^N) = 1.5(e_d^P i_d^N + e_q^P i_q^N + e_d^N i_d^P + e_q^N i_q^P) \\
p_{s2} = 1.5(E_{dq}^N \otimes I_{dq}^P - E_{dq}^P \otimes I_{dq}^N) = 1.5(e_q^N i_d^P - e_d^N i_q^P - e_q^P i_d^N + e_d^P i_q^N) \\
q_0 = 1.5(E_{dq}^P \otimes I_{dq}^P + E_{dq}^N \otimes I_{dq}^N) = 1.5(e_q^P i_d^P - e_d^P i_q^P + e_q^N i_d^N - e_d^N i_q^N) \\
q_{c2} = 1.5(E_{dq}^N \otimes I_{dq}^P + E_{dq}^P \otimes I_{dq}^N) = 1.5(e_q^P i_d^N - e_d^P i_q^N + e_q^N i_d^P - e_d^N i_q^P) \\
q_{s2} = 1.5(-E_{dq}^N \odot I_{dq}^P + E_{dq}^P \odot I_{dq}^N) = 1.5(e_q^P i_d^N + e_d^P i_q^N - e_q^N i_d^P - e_d^N i_q^P)
\end{cases}
\tag{8}
$$

where, e_d^P and e_q^P are the projection of E_{dq}^P on the dq axis respectively. e_d^N and e_q^N are respectively the projection of E_{dq}^N on the dq axis. i_d^P and i_q^P are the projection of I_{dq}^P on the dq axis. i_d^N and i_q^N are the projection of I_{dq}^N on the dq axis.

Equation (8) shows I only contains four components $(i_d^P, i_q^P, i_d^N, i_q^N)$ under unbalanced grid conditions, which cannot meet the control requirements of the six components of instantaneous power at the same time. If the control objective is to suppress the second harmonic component of p, the q will contain the second harmonic component, and the traditional FCS-MPDPC will not be applicable.

2.2. New Instantaneous Power in dq Coordinate System

To solve above problems, the new instantaneous power theory is used [22]. In the new instantaneous power, the instantaneous active power is equivalent to the traditional instantaneous active power, but the new instantaneous reactive power is:

$$
q^{nov} = 1.5 Re(I^* E')
\tag{9}
$$

where, E' is the vector with 90° lag E, which is:

$$
E' = -jE_{dq}^P e^{j\omega t} + jE_{dq}^N e^{-j\omega t}
\tag{10}
$$

Thus, the q^{nov} can be deduced as:

$$
q^{nov}(t) = q_0^{nov} + q_{c2}^{nov} \cos(2\omega t) + q_{s2}^{nov} \sin(2\omega t)
\tag{11}
$$

where,

$$
\begin{cases}
q_0^{nov} = 1.5(E_{dq}^P \otimes I_{dq}^P - E_{dq}^N \otimes I_{dq}^N) = 1.5(e_q^P i_d^P - e_d^P i_q^P - e_q^N i_d^N + e_d^N i_q^N) \\
q_{c2}^{nov} = 1.5(-E_{dq}^N \otimes I_{dq}^P + E_{dq}^P \otimes I_{dq}^N) = 1.5(e_d^N i_q^P - e_q^N i_d^P + e_q^P i_d^N - e_d^P i_q^N) \\
q_{s2}^{nov} = 1.5(E_{dq}^N \odot I_{dq}^P + E_{dq}^P \odot I_{dq}^N) = 1.5(e_d^N i_d^P + e_q^N i_q^P + e_q^P i_d^N + e_q^P i_q^N)
\end{cases}
\tag{12}
$$

By comparing Equation (8) with Equation (12), it can be seen that $p_{c2} = q_{s2}^{nov}$ and $p_{s2} = -q_{c2}^{nov}$. When the instantaneous active power output of PWM rectifier has no pulsation component, the instantaneous reactive power output also has no pulsation component, which can realize the new instantaneous power are constant under the condition of unbalanced power grid.

3. New FCS-MPDPC

The new instantaneous power in the $\alpha\beta$ coordinate system is:

$$
\begin{bmatrix} p \\ q^{nov} \end{bmatrix} = 1.5 \begin{bmatrix} e_\alpha & e_\beta \\ e_\alpha' & e_\beta' \end{bmatrix} \begin{bmatrix} i_\alpha \\ i_\beta \end{bmatrix}
\tag{13}
$$

where, e'_α and e'_β are the components of E'.

According to Equation (13), the change rate of the new instantaneous power is:

$$\begin{cases} \frac{dp}{dt} = 1.5 \left(\frac{de_\alpha}{dt} i_\alpha + e_\alpha \frac{di_\alpha}{dt} + \frac{de_\beta}{dt} i_\beta + e_\beta \frac{di_\beta}{dt} \right) \\ \frac{dq^{nov}}{dt} = 1.5 \left(\frac{de'_\alpha}{dt} i_\alpha + e'_\alpha \frac{di_\alpha}{dt} + \frac{de'_\beta}{dt} i_\beta + e'_\beta \frac{di_\beta}{dt} \right) \end{cases} \tag{14}$$

Under unbalanced power grid condition, the differential form of E is:

$$\frac{dE}{dt} = j\omega E^P_{dq} e^{j\omega t} - j\omega E^N_{dq} e^{-j\omega t} \tag{15}$$

Substituting Equation (4) into Equation (15) obtains:

$$\frac{dE}{dt} = -\omega E' \tag{16}$$

According to Equation (16), the rate of change of α and β components of E in the static $\alpha\beta$ coordinate system is:

$$\begin{cases} \frac{de_\alpha}{dt} = -\omega e'_\alpha \\ \frac{de_\beta}{dt} = -\omega e'_\beta \end{cases} \tag{17}$$

Similarly, the rate of change of E' in the $\alpha\beta$ coordinate system is:

$$\begin{cases} \frac{de'_\alpha}{dt} = \omega e_\alpha \\ \frac{de'_\beta}{dt} = \omega e_\beta \end{cases} \tag{18}$$

Combined with Equations (3), (14), (17) and (18), the differential expression of the new instantaneous power can be written as:

$$\begin{cases} \frac{dp}{dt} = \frac{1.5}{L} \left(e^2_\alpha + e^2_\beta - e_\alpha v_\alpha - e_\beta v_\beta \right) - \frac{R}{L} p - \omega q^{nov} \\ \frac{dq^{nov}}{dt} = \frac{1.5}{L} \left(e_\alpha e'_\alpha + e_\beta e'_\beta - v_\alpha e'_\alpha - v_\beta e'_\beta \right) - \frac{R}{L} q^{nov} + \omega p \end{cases} \tag{19}$$

According to Equation (19), the change rate under the action of each voltage vector is calculated as follows:

$$\begin{cases} s_{pi} = \frac{dp}{dt} \Big| (V_i) = \frac{1.5}{L} \left(e^2_\alpha + e^2_\beta - e_\alpha v_{\alpha-i} - e_\beta v_{\beta-i} \right) - \frac{R}{L} p - \omega q^{nov} \\ s_{qi} = \frac{dq^{nov}}{dt} \Big| (V_i) = \frac{1.5}{L} \left(e_\alpha e'_\alpha + e_\beta e'_\beta - v_{\alpha-i} e'_\alpha - v_{\beta-i} e'_\beta \right) - \frac{R}{L} q^{nov} + \omega p \end{cases} \quad i \in [0,7] \tag{20}$$

Figure 2 shows the change of instantaneous power rate with the phase Angle of E under the action of eight different voltage vectors (V_0–V_7). As can be seen from Figure 2, in the case of grid unbalance, the instantaneous power change rate corresponding to the two zero voltage vectors is not constant, but a pulsating component.
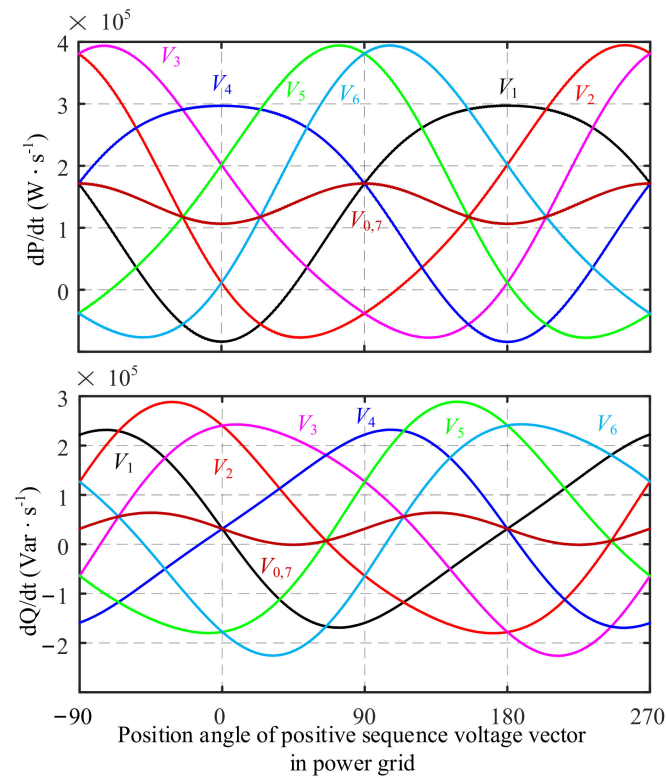
Figure 2. New instantaneous power slopes of various rectifier voltage vectors.

To achieve the goal that the new instantaneous power output of the PWM rectifier follows the given value; the objective function is composed of the error term of this new instantaneous power and the given value. The objective function is:

$$cf = \left(p_{ref} - p_{k+1}\right)^2 + \left(q^{nov}_{ref} - q^{nov}_{k+1}\right)^2 \tag{21}$$

In the Equation (21), p_{k+1} and q^{nov}_{k+1} are the predicted values of p and q^{nov} in the next control period, respectively. p_{ref} and q^{nov}_{ref} are given values, respectively.

A three-vector FCS-MPDPC is proposed, in a control cycle one zero vector and two adjacent non-zero voltage vectors are selected. There are six different combination modes of two non-zero vectors, namely $\{V_1, V_2\}$, $\{V_2, V_3\},\ldots, \{V_6, V_1\}$. Based on the three voltage vectors, the control system needs to select the most suitable group from these six combinations, and generate six PWM control signals, according to the action time and action sequence of each vector.

The selection and the calculation of action time of the vector occur at the same time. Before the most suitable vector combination is obtained, the action time of each vector needs to be calculated, and then the instantaneous power of the next control cycle corresponding to the vector combination is predicted. Finally, the most suitable voltage vector combination is selected by the smallest objective function.

Assuming that the optimal non-zero vector combination in a current control cycle is $\{V_1, V_2\}$. V_0 is the zero vector, the vector combination used by the control system is $\{V_1, V_2, V_0\}$. The change rates of instantaneous active power corresponding to the voltage vector combination $\{V_1, V_2, V_0\}$ are s_{p1}, s_{p2}, and s_{p0}, respectively, and the corresponding instantaneous reactive power change rates are s_{q1}, s_{q2}, s_{q0}, then the instantaneous rate in the next control cycle. The predicted value of power is as follows:

$$\begin{cases} p_{k+1} = p_k + s_{p1} \cdot t_1 + s_{p2} \cdot t_2 + s_{p0} \cdot (T_s - t_1 - t_2) \\ q_{k+1} = q_k + s_{q1} \cdot t_1 + s_{q2} \cdot t_2 + s_{q0} \cdot (T_s - t_1 - t_2) \end{cases} \tag{22}$$

where, T_s means the control period. t_1 and t_2 are the action time of V_1 and V_2, respectively.

Since the control goal of model prediction is to minimize *cf*, the minimum *cf* in Equation (21) is used as the constraint condition, the time of each non-zero vector should satisfy:

$$\begin{cases} \dfrac{\partial cf}{\partial t_1} = 0 \\ \dfrac{\partial cf}{\partial t_2} = 0 \end{cases} \tag{23}$$

By solving the Equation (23), the action time of V_1 and V_2 was found to be:

$$\begin{cases} t_1 = \dfrac{\left(s_{q2}-s_{q0}\right)\left(p_{ref}-p_{k+1}\right)+\left(s_{p0}-s_{p2}\right)\left(q_{ref}-q_{k+1}\right)+\left(s_{q0}s_{p2}-s_{q2}s_{p0}\right)T_s}{\left(s_{q2}-s_{q0}\right)s_{p1}-\left(s_{q1}-s_{q0}\right)s_{p2}-\left(s_{q2}-s_{q1}\right)s_{p0}} \\ t_2 = \dfrac{\left(s_{q0}-s_{q1}\right)\left(p_{ref}-p_{k+1}\right)+\left(s_{p1}-s_{p0}\right)\left(q_{ref}-q_{k+1}\right)+\left(s_{q1}s_{p0}-s_{q0}s_{p1}\right)T_s}{\left(s_{q2}-s_{q0}\right)s_{p1}-\left(s_{q1}-s_{q0}\right)s_{p2}-\left(s_{q2}-s_{q1}\right)s_{p0}} \end{cases} \tag{24}$$

After obtaining the action time t_1 and t_2, when t_1 or t_2 is less than zero, then t_1 or t_2 is equal to zero; when t_1 or t_2 is greater than T_s, then t_1 or t_2 is equal to T_s. After simply processing t_1 and t_2 of the non-zero voltage vector, when $t_1 + t_2 > T_s$, the action time t_0, t_1 and t_2 should be adjusted to:

$$\begin{cases} t_1 = \dfrac{t_1}{t_1+t_2}T_s \\ t_2 = \dfrac{t_2}{t_1+t_2}T_s \\ t_0 = T_s - t_1 - t_2 \end{cases} \tag{25}$$

Substituting Equation (25) into Equation (22), the predicted value of instantaneous power under the action of the voltage vector combination $\{V_1, V_2, V_0\}$ can be calculated. Then combine Equation (21) to get the corresponding objective function value cf_1. In the same way, the values cf_2, cf_3,..., cf_6 of the objective function under the action of other vector combinations can be calculated. To minimize the instantaneous power error, the voltage vector combination corresponding to the minimum *cf* is the optimal voltage vector combination. When the optimal voltage vector combination is determined, it can be modulated according to the SVPWM method.

Figure 3 is the new FCS-MPDPC control diagram, which is mainly divided into six key links, such as delay vector solution, new instantaneous power calculation, new instantaneous power prediction, objective function optimization, voltage vector selection and operation time calculation and pulse width modulation.
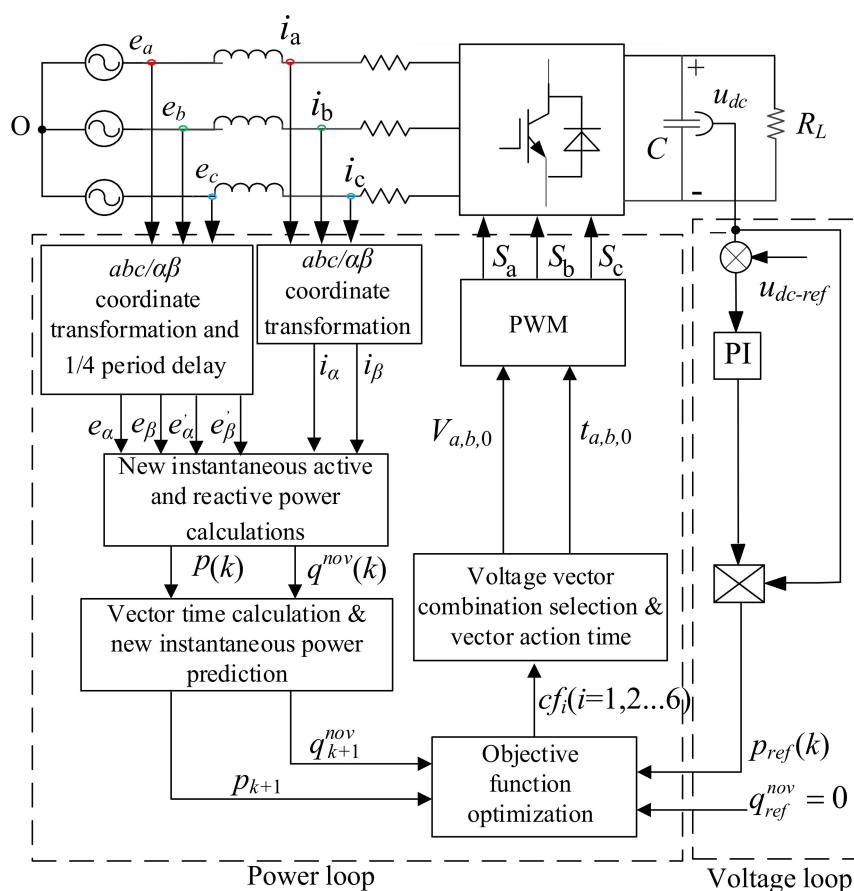
Figure 3. Control diagram of novel FCS-MPDPC.

4. Simulation and Experimental

To verify the effectiveness of the new FCS-MPDPC, and an experimental platform is built. In addition, this paper also compares and analyzes the three-vector FCS-MPDPC in the reference [19]. The sampling frequency of the two methods is 10 kHz. Table 1 indicates the parameters of the control system. In order to create the unbalanced situation of three-phase power grid, 3 Ω unbalanced resistors are connected in series in the A-phase loop of PWM rectifier.

Table 1. The parameters of control system.

Parameter	Value
DC bus voltage u_{dc}/V	60
Phase voltage of three-phase network E_{rms}/V	20
Grid rated frequency f/Hz	50
Grid side filter inductor L/mH	7
DC side capacitance $C/\mu F$	600
DC side load resistance R/Ω	36.5
Sampling frequency f/Hz	10,000

4.1. The Simulation

In the Matlab 2021a of MathWorks, the traditional and new FCS-MPDPC simulation models are built, and the simulation results are analyzed.

Under unbalanced power grid conditions, the sinusoidal degree of three-phase current waveforms in the traditional FCS-MPDPC is low, as shown in Figures 4 and 5, especially where the A-phase current waveform is seriously distorted, the three-phase current is

asymmetric, and the instantaneous power has pulsating components. According to the spectrum analysis of A-phase current, in Figure 6, the THD of A-phase current is 7.13%, which cannot be obtained to meet the requirements of PWM rectifier grid-connected control; the amplitude of fundamental current is 2.812 A. In addition, there are many low-order harmonics, especially the third and fifth harmonics. Therefore, under unbalanced three-phase power grid condition, if the traditional FCS-MPDPC is adopted, the harmonic content of three-phase power grid current is high, which will cause certain "pollution" to the power grid.
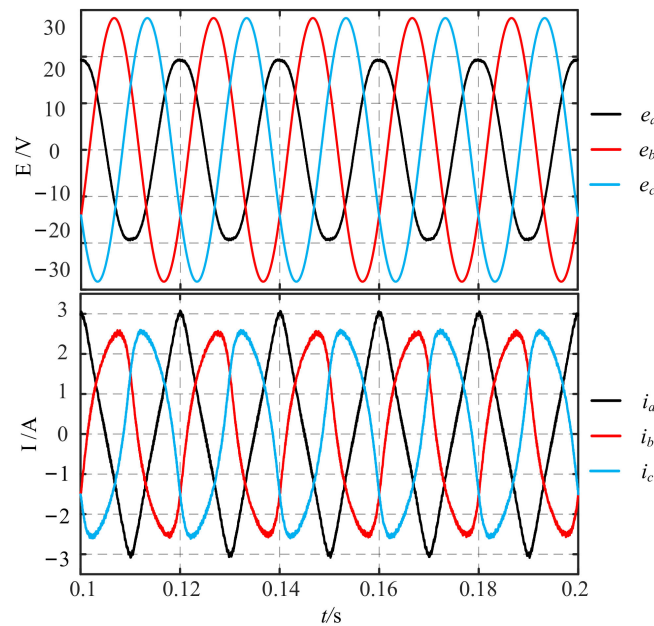
Figure 4. Waveforms of conventional FCS-MPDPC.
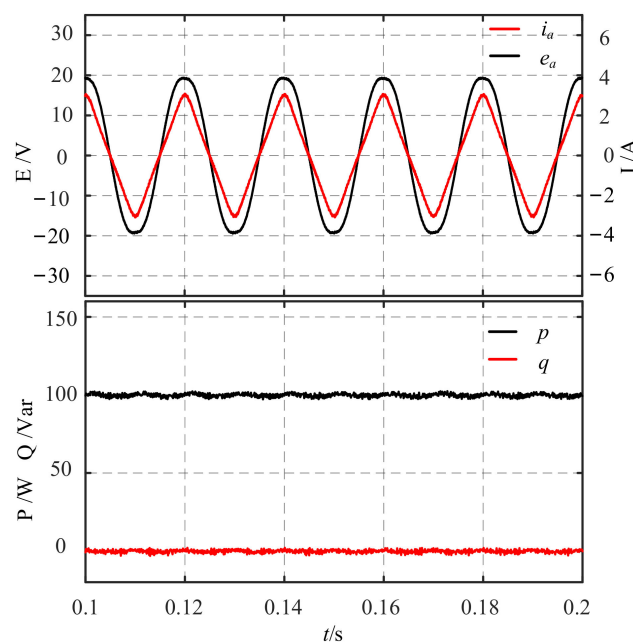
Figure 5. Instantaneous power waveform of conventional FCS-MPDPC.

Fundamental (50Hz) = 2.812 , THD= 7.13%
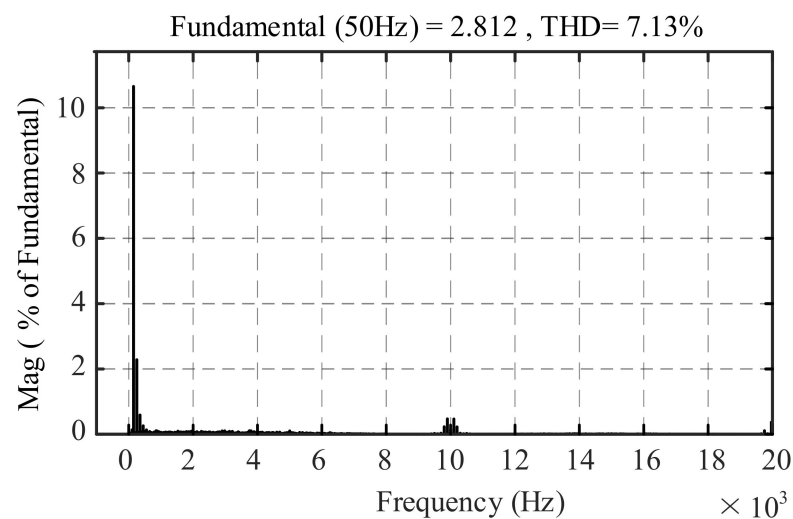
Figure 6. Spectrum analysis of A-phase current of conventional FCS-MPDPC.

It can be seen from Equations (7) and (11), if the second harmonic of DC side voltage is to be suppressed, p_{c2} and p_{s2} must be suppressed, but q_{c2} and q_{s2} cannot be eliminated, that is, the instantaneous reactive power is not a constant value, but a sinusoidal pulsating component. The unbalanced control method for suppressing the second harmonic component, only the control signal of instantaneous active power can be a fixed value or step command, and the instantaneous reactive power can only be sinusoidal pulsating component.

On the contrary, the new FCS-MPDPC has good steady-state performance. In Figures 7 and 8, the current waveform of three-phase power grid is highly sinusoidal, voltage and current are in the same phase, and the new type of instantaneous power pulsation is small. By analyzing the spectrum of A-phase current, shown in Figure 9, the amplitude of fundamental current is 2.997 A; the THD of current is only 0.97%, which significantly reduces the low-order harmonic component of current, and the high-order harmonic is mainly concentrated in the integral multiple of switching frequency. The filter inductor is simple in design.
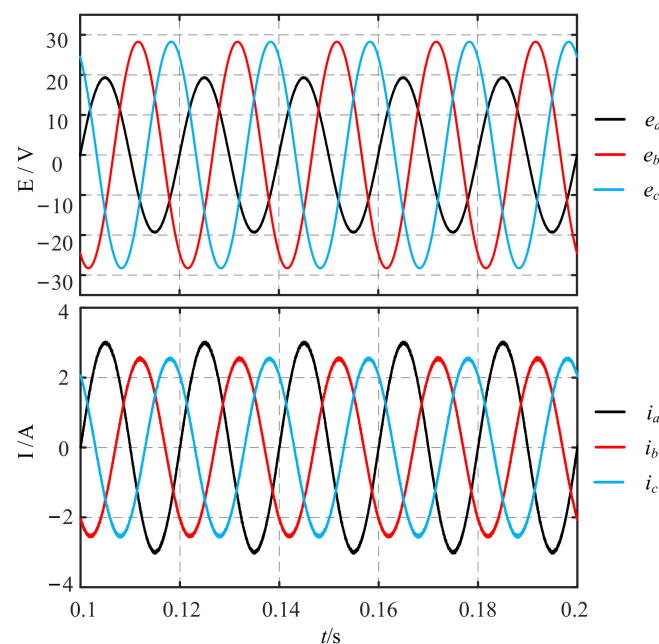
Figure 7. Waveforms of novel FCS-MDPC of novel FCS-MDPC.
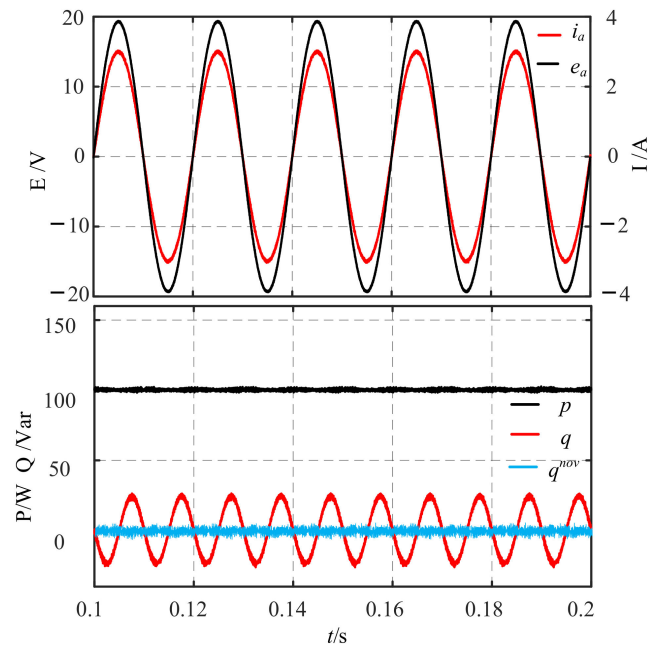
Figure 8. Instantaneous power and new instantaneous power waveform.
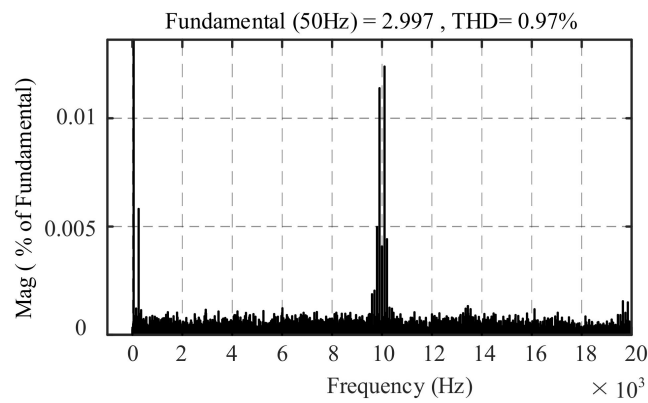
Figure 9. Spectrum analysis of A-phase current of novel FCS-MDPC.

4.2. The Experiment

The experiments were carried out on the experimental platform, as shown in Figure 10.
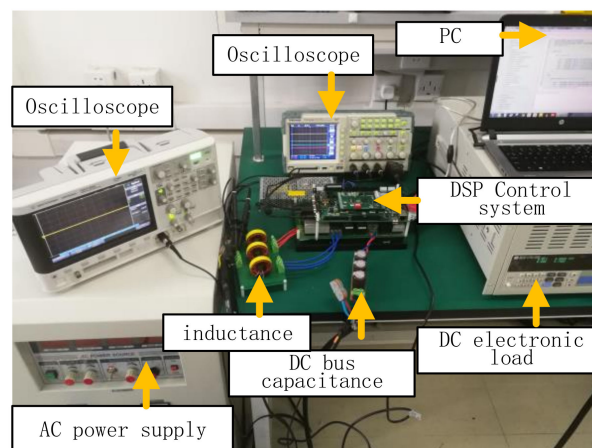
Figure 10. Two-level three-phase PWM rectifier experimental platform.

Figures 11 and 12, respectively, show the experimental results of traditional and new FCS-MPDPC under power grid unbalance condition. In Figure 11, waveforms of the three-phase current in the traditional FCS-MPDPC is seriously distorted; especially the A-phase current waveform is approximately triangular. Further spectrum analysis of the three-phase current shows that THD of the three-phase current is 6.374%, 5.865% and 5.835%, respectively, which cannot meet the requirements of current THD of PWM rectifier grid-connected control [23].

(a)

I1 — fPLL1:I1 50.006 Hz

Order	I1 [A]	hdf[%]		Order	I1 [A]	hdf[%]	Order	I1 [A]	hdf[%]
	Total	1.6254		dc	-------	-------			
	1	1.6221	99.797	2	0.0214	1.315			
	3	0.0999	6.149	4	0.0077	0.474			
Urms1	14.708 V	5	0.0144	0.889	6	0.0005	0.029		
Irms1	1.6230 A	7	0.0023	0.144	8	0.0030	0.187		
P1	23.770 W	9	0.0002	0.015	10	0.0003	0.016		
S1	23.871 VA	11	0.0002	0.010	12	0.0007	0.043		
Q1	2.188 var	13	0.0002	0.010	14	0.0004	0.022		
λ1	0.9958	15	0.0002	0.010	16	0.0003	0.019		
Φ1	65.26 °	17	0.0002	0.013	18	0.0002	0.014		
		19	0.0001	0.009	20	0.0001	0.004		
Uthd1	2.410 %	21	0.0002	0.011	22	0.0001	0.009		
Ithd1	6.374 %	23	0.0003	0.021	24	0.0004	0.025		
Pthd1	0.153 %	25	0.0002	0.015	26	0.0001	0.004		
Uthf1	0.198 %	27	0.0003	0.020	28	0.0001	0.008		
Ithf1	0.135 %	29	0.0003	0.018	30	0.0002	0.013		
Utif1	8.625	31	0.0001	0.006	32	0.0001	0.009		
Itif1	4.689	33	0.0001	0.007	34	0.0001	0.008		
hvf1	1.396 %	35	0.0001	0.008	36	0.0002	0.010		
hcf1	3.700 %	37	0.0001	0.005	38	0.0001	0.007		
Kfact1	1.0340	39	0.0001	0.004	40	0.0001	0.005		

I2 — fPLL1:I1 50.006 Hz

	Order	I2 [A]	hdf[%]	Order	I2 [A]	hdf[%]
	Total	1.4687		dc	-------	-------
	1	1.4661	99.828	2	0.0064	0.436
	3	0.0852	5.799	4	0.0070	0.476
Urms2	19.632 V	5	0.0077	0.523	6	0.0027	0.181
Irms2	1.4673 A	7	0.0017	0.118	8	0.0019	0.128
P2	28.734 W	9	0.0007	0.050	10	0.0008	0.057
S2	28.807 VA	11	0.0005	0.036	12	0.0005	0.033
Q2	2.045 var	13	0.0002	0.015	14	0.0003	0.021
λ2	0.9975	15	0.0002	0.010	16	0.0002	0.011
Φ2	64.07 °	17	0.0000	0.001	18	0.0002	0.017
		19	0.0002	0.012	20	0.0000	0.003
Uthd2	0.197 %	21	0.0002	0.015	22	0.0001	0.006
Ithd2	5.865 %	23	0.0003	0.018	24	0.0002	0.011
Pthd2	0.008 %	25	0.0002	0.011	26	0.0002	0.015
Uthf2	0.141 %	27	0.0002	0.015	28	0.0002	0.016
Ithf2	0.215 %	29	0.0003	0.022	30	0.0002	0.017
Utif2	6.127	31	0.0003	0.023	32	0.0004	0.029
Itif2	8.990	33	0.0005	0.036	34	0.0005	0.035
hvf2	0.101 %	35	0.0005	0.036	36	0.0005	0.035
hcf2	3.380 %	37	0.0006	0.039	38	0.0004	0.029
Kfact2	1.0305	39	0.0004	0.029	40	0.0003	0.021

I3 — fPLL1:I1 50.006 Hz

	Order	I3 [A]	hdf[%]	Order	I3 [A]	hdf[%]
	Total	1.5073		dc	-------	-------
	1	1.5048	99.830	2	0.0154	1.020
	3	0.0850	5.639	4	0.0085	0.564
Urms3	19.722 V	5	0.0133	0.884	6	0.0030	0.202
Irms3	1.5062 A	7	0.0026	0.176	8	0.0014	0.091
P3	29.556 W	9	0.0010	0.063	10	0.0008	0.054
S3	29.706 VA	11	0.0005	0.036	12	0.0010	0.063
Q3	2.980 var	13	0.0001	0.008	14	0.0004	0.024
λ3	0.9950	15	0.0000	0.003	16	0.0003	0.019
Φ3	65.76 °	17	0.0003	0.017	18	0.0002	0.011
		19	0.0002	0.012	20	0.0000	0.003
Uthd3	0.228 %	21	0.0001	0.004	22	0.0001	0.009
Ithd3	5.835 %	23	0.0001	0.009	24	0.0003	0.022
Pthd3	0.009 %	25	0.0002	0.013	26	0.0002	0.014
Uthf3	0.169 %	27	0.0002	0.013	28	0.0003	0.018
Ithf3	0.232 %	29	0.0006	0.041	30	0.0002	0.013
Utif3	7.709	31	0.0004	0.028	32	0.0004	0.028
Itif3	9.557	33	0.0006	0.038	34	0.0005	0.032
hvf3	0.118 %	35	0.0008	0.051	36	0.0006	0.037
hcf3	3.372 %	37	0.0005	0.032	38	0.0004	0.025
Kfact3	1.0309	39	0.0004	0.027	40	0.0002	0.015

(b)

Figure 11. Experimental results of conventional FCS-MPDPC under unbalanced grid voltages; (**a**) voltage and current waveforms; (**b**) spectrum analysis of current.

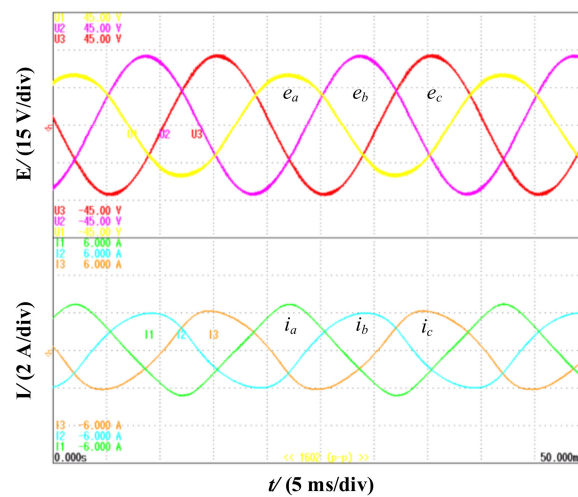Under the unbalanced three-phase power grid condition, if the traditional FCS-MPDPC is adopted, the harmonic content of three-phase current will be too much, especially the third and fifth harmonics, which will cause certain interference to the power grid.

On the contrary, the new FCS-MPDPC has good steady-state performance. In Figure 12, current waveforms of the three-phase grid has high sinusoidal degree and fewer burrs. Voltage and current are in the same phase. From spectrum analysis of three-phase current, the THD of three-phase current is 0.902%, 0.812% and 0.843%, respectively, which is about 1/7 of the three-phase current THD in traditional FCS-MPDPC. Therefore, compared with the traditional FCS-MPDPC, under grid unbalance conditions, the new FCS-MPDPC can suppress the harmonic component of the current on the grid side and improve the performance of the control system.

In addition, this paper also verifies the effectiveness of the new FCS-MPDPC under three-phase power grid balance. Figure 13 shows the experimental results. Figure 13a shows that the new FCS-MPDPC can suppress the harmonic component of the current and

reduce the instantaneous active and reactive power pulsation. In Figure 13b, when the new instantaneous active power changes from 70 W to 140 W, FCS-MPDPC can quickly track the change of the given value while keeping the new instantaneous reactive power. The harmonic analysis of current shows that the THD is small. The low order harmonic content is less, and the high order harmonic is mainly concentrated on the integral multiple of the switching frequency, which is conducive to the filtering of high order harmonic components. It has good dynamic response performance.
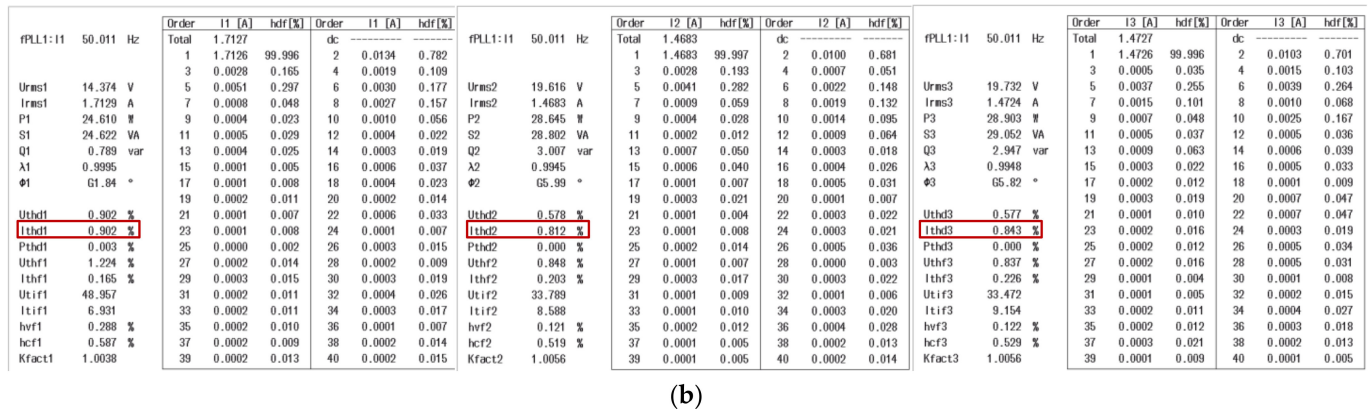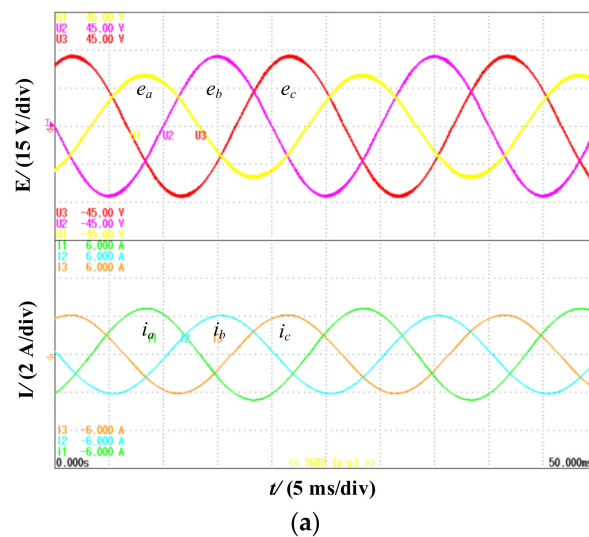
E/ (15 V/div) — e_a, e_b, e_c

I/ (2 A/div) — i_a, i_b, i_c

t/ (5 ms/div)

(a)

Panel 1

fPLL1:I1 50.011 Hz

Urms1	14.374	V
Irms1	1.7129	A
P1	24.610	W
S1	24.622	VA
Q1	0.789	var
λ1	0.9995	
Φ1	G1.84	°
Uthd1	0.902	%
Ithd1	0.902	%
Pthd1	0.003	%
Uthf1	1.224	%
Ithf1	0.165	%
Utif1	48.957	
Itif1	6.931	
hvf1	0.288	%
hcf1	0.587	%
Kfact1	1.0038	

Order	I1 [A]	hdf [%]	Order	I1 [A]	hdf [%]
Total	1.7127		dc		
1	1.7126	99.996	2	0.0134	0.782
3	0.0028	0.165	4	0.0019	0.109
5	0.0051	0.297	6	0.0030	0.177
7	0.0008	0.048	8	0.0027	0.157
9	0.0004	0.023	10	0.0010	0.056
11	0.0005	0.029	12	0.0004	0.022
13	0.0004	0.025	14	0.0003	0.019
15	0.0001	0.005	16	0.0006	0.037
17	0.0001	0.008	18	0.0004	0.023
19	0.0002	0.011	20	0.0002	0.014
21	0.0001	0.007	22	0.0006	0.033
23	0.0001	0.008	24	0.0001	0.007
25	0.0000	0.002	26	0.0003	0.015
27	0.0002	0.014	28	0.0002	0.009
29	0.0003	0.015	30	0.0003	0.019
31	0.0002	0.011	32	0.0004	0.026
33	0.0002	0.011	34	0.0003	0.017
35	0.0002	0.010	36	0.0001	0.007
37	0.0002	0.009	38	0.0002	0.014
39	0.0002	0.013	40	0.0002	0.015

Panel 2

fPLL1:I1 50.011 Hz

Urms2	19.616	V
Irms2	1.4683	A
P2	28.645	W
S2	28.802	VA
Q2	3.007	var
λ2	0.9945	
Φ2	G5.99	°
Uthd2	0.578	%
Ithd2	0.812	%
Pthd2	0.000	%
Uthf2	0.848	%
Ithf2	0.203	%
Utif2	33.789	
Itif2	8.588	
hvf2	0.121	%
hcf2	0.519	%
Kfact2	1.0056	

Order	I2 [A]	hdf [%]	Order	I2 [A]	hdf [%]
Total	1.4683		dc		
1	1.4683	99.997	2	0.0100	0.681
3	0.0028	0.193	4	0.0007	0.051
5	0.0041	0.282	6	0.0022	0.148
7	0.0009	0.059	8	0.0019	0.132
9	0.0004	0.028	10	0.0014	0.095
11	0.0002	0.012	12	0.0009	0.064
13	0.0007	0.050	14	0.0003	0.018
15	0.0006	0.040	16	0.0004	0.026
17	0.0001	0.007	18	0.0005	0.031
19	0.0003	0.021	20	0.0001	0.007
21	0.0001	0.004	22	0.0003	0.022
23	0.0001	0.008	24	0.0003	0.021
25	0.0002	0.014	26	0.0005	0.036
27	0.0001	0.007	28	0.0000	0.003
29	0.0003	0.017	30	0.0003	0.022
31	0.0001	0.009	32	0.0001	0.006
33	0.0001	0.010	34	0.0003	0.020
35	0.0002	0.012	36	0.0004	0.028
37	0.0001	0.005	38	0.0002	0.013
39	0.0001	0.005	40	0.0002	0.014

Panel 3

fPLL1:I1 50.011 Hz

Urms3	19.732	V
Irms3	1.4724	A
P3	28.903	W
S3	29.052	VA
Q3	2.947	var
λ3	0.9948	
Φ3	G5.82	°
Uthd3	0.577	%
Ithd3	0.843	%
Pthd3	0.000	%
Uthf3	0.837	%
Ithf3	0.226	%
Utif3	33.472	
Itif3	9.154	
hvf3	0.122	%
hcf3	0.529	%
Kfact3	1.0056	

Order	I3 [A]	hdf [%]	Order	I3 [A]	hdf [%]
Total	1.4727		dc		
1	1.4726	99.996	2	0.0103	0.701
3	0.0005	0.035	4	0.0015	0.103
5	0.0037	0.255	6	0.0039	0.264
7	0.0015	0.101	8	0.0010	0.068
9	0.0007	0.048	10	0.0025	0.167
11	0.0005	0.037	12	0.0005	0.036
13	0.0009	0.063	14	0.0006	0.039
15	0.0003	0.022	16	0.0005	0.033
17	0.0002	0.012	18	0.0001	0.009
19	0.0003	0.019	20	0.0007	0.047
21	0.0001	0.010	22	0.0007	0.047
23	0.0002	0.016	24	0.0003	0.019
25	0.0002	0.012	26	0.0005	0.034
27	0.0002	0.016	28	0.0005	0.031
29	0.0001	0.004	30	0.0001	0.008
31	0.0001	0.005	32	0.0002	0.015
33	0.0002	0.011	34	0.0004	0.027
35	0.0002	0.012	36	0.0003	0.018
37	0.0003	0.021	38	0.0002	0.013
39	0.0001	0.009	40	0.0001	0.005

(b)

Figure 12. Experimental results of novel FCS-MPDPC under unbalanced grid voltages; (**a**) voltage and current waveforms; (**b**) spectrum analysis of current.
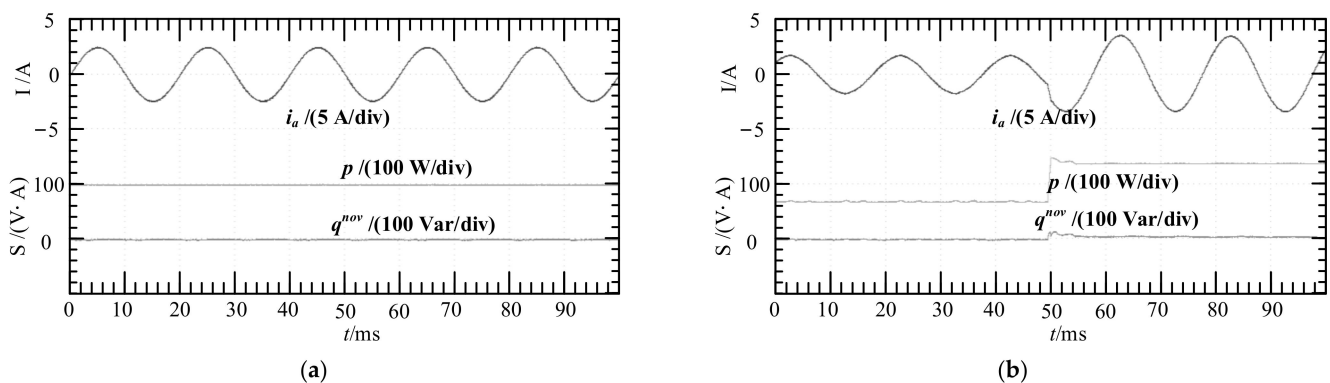
[Left plot] I /A ; S /(V·A) ; i_a /(5 A/div) ; p /(100 W/div) ; q^{nov} /(100 Var/div) ; t/ms

(a)

[Right plot] I /A ; S /(V·A) ; i_a /(5 A/div) ; p /(100 W/div) ; q^{nov} /(100 Var/div) ; t/ms

(b)

Figure 13. Experimental results of novel FCS-MPDPC under balanced grid voltages; (**a**) steady-state waveform; (**b**) dynamic waveforms.

5. Conclusions

A novel three vector three-phase voltage source PWM rectifier FCS-MPDPC is presented. Under the unbalanced power grid condition, compared with the traditional method, FCS-MPDPC proposed adopts the new instantaneous power theory, redefines the instantaneous reactive power. This method can effectively suppress the harmonic component of current and reduce the instantaneous active power pulsation, which has the advantages of low harmonic content of current on the grid side, fixed switching frequency and small instantaneous power pulsation. Therefore, the new FCS-MPDPC is a control strategy with great practical value.

Author Contributions: Conceptualization, L.T. and M.L.; methodology, L.T. and H.L.; software, L.T.; validation, L.T., H.L. and Y.L.; formal analysis, L.T.; writing—original draft preparation, L.T.; writing—review and editing, M.L.; visualization, H.L. and Y.L. All authors have read and agreed to the published version of the manuscript.

Conflicts of Interest: The authors declare no conflict of interest.

Abbreviations

MPDPC	Model predictive direct power control
PWM	Pulse-width modulation
MPC	Model predictive control
FCS-MPDPC	Finite control set model predictive direct power control
THD	Total harmonic distortion

References

1. Tarisciotti, L.; Zanchetta, P.; Watson, A.; Clare, J.; Degano, M.; Bifaretti, S. Modulated model predictive control (M2PC) for a 3-phase active front-end. In Proceedings of the 2013 IEEE Energy Conversion Congress and Exposition, Denver, CO, USA, 15–19 September 2013; pp. 1062–1069.
2. Rivera, M. A new predictive control scheme for a VSI with reduced common mode voltage operating at fixed switching frequency. In Proceedings of the 2015 IEEE 5th International Conference on Power Engineering, Energy and Electrical Drives (POWERENG), Riga, Latvia, 11–13 May 2015; pp. 617–622.
3. Riar, B.S.; Scoltock, J.; Madawala, U.K. Model predictive direct slope control for power converters. *IEEE Trans. Power Electron.* **2017**, *32*, 2278–2289. [CrossRef]
4. Arif, B.; Tarisciotti, L.; Zanchetta, P. Grid parameter estimation using model predictive direct power control. *IEEE Trans. Ind. Appl.* **2015**, *51*, 4614–4622. [CrossRef]
5. Cortés, P.; Rodriguez, J.; Antoniewicz, P.; Kazmierkowski, M. Direct Power Control of an AFE Using Predictive Control. *IEEE Trans. Power Electron.* **2008**, *23*, 2516–2523. [CrossRef]
6. Zhang, Y.; Xie, W.; Li, Z.; Zhang, Y. Model Predictive Direct Power Control of a PWM Rectifier with Duty Cycle Optimization. *IEEE Trans. Power Electron.* **2013**, *28*, 5343–5351. [CrossRef]
7. Shang, L.; Sun, D. Predictive direct power control of three-Phase grid-connected voltage-sourced inverters. *Trans. China Electrotech. Soc.* **2011**, *26*, 216–222.
8. Song, Z.; Chen, W.; Xia, C. Predictive direct power control for three-phase grid-connected converters without sector information and voltage vector selection. *IEEE Trans. Power Electron.* **2014**, *29*, 5518–5531. [CrossRef]
9. Bouafia, A.; Gaubert, J.; Krim, F. Predictive direct power control of three-phase PWM rectifier using SVM. *IEEE Trans. Power Electron.* **2010**, *25*, 228–236. [CrossRef]
10. Ding, W.; Pan, Z. A new predictive direct power control solution for three-phase grid-connected inverters. *Trans. China Electrotech. Soc.* **2015**, *30*, 67–74.
11. Tao, Y.; Wu, Q.; Wang, L.; Tang, W. Voltage sensorless predictive direct power control of three-phase PWM converters. *IET Power Electron.* **2016**, *9*, 1009–1018. [CrossRef]
12. Shen, S.; Zhou, Y. UPFC control strategy based on improved predictive direct power control. *Guangdong Electr. Power* **2018**, *31*, 93–98.
13. Tang, N.; Xiao, X. Direct power control for sliding mode variable structure of permanent-magnet direct drive wind power generator. *Guangdong Electr. Power* **2013**, *26*, 64–69.

14. Han, Y.; Lin, M.; Hao, L. Triple-state direct power control strategy of three-phase boost type PWM rectifiers. *Trans. China Electrotech. Soc.* **2013**, *28*, 208–212.

15. Yao, X.; Wang, X. Research on double switching vector table direct power control of three-phase voltage source PWM rectifier. *Electr. Mach. Control.* **2015**, *19*, 71–77.

16. Zhang, Y.; Qu, C.; Li, Z.; Xu, W. Model predictive control and direct power control for PWM rectifiers with active power ripple minimization. *IEEE Trans. Ind. Appl.* **2016**, *52*, 4909–4918. [CrossRef]

17. Choi, D.; Lee, K. Dynamic performance improvement of AC/DC converter using model predictive direct power control with finite control set. *IEEE Trans. Ind. Electron.* **2015**, *62*, 757–767. [CrossRef]

18. Zhang, Z.; Feng, X.; Fang, H. Ripple-reduced model predictive direct power control for active front-end power converters with extended switching vectors and time-optimized control. *IET Power Electron.* **2016**, *9*, 1914–1923.

19. Li, H.; Lin, M.; Ai, J.; Yang, G.; Wang, X.; Le, W. Three-Vector-Based Model Predictive Direct Power Control Strategy for PWM Rectifier. In Proceedings of the 2018 IEEE Energy Conversion Congress and Exposition (ECCE), Portland, OR, USA, 23–27 September 2018; pp. 4039–4045.

20. Vazquez, S.; Marquez, A.; Aguilera, R.P.; Quevedo, D.E.; Leon, J.I.; Franquelo, L.G. Predictive Optimal Switching Sequence Direct Power Control for Grid-Connected Power Converters. *IEEE Trans. Ind. Electron.* **2015**, *62*, 757–767. [CrossRef]

21. Akagi, H.; Kanazawa, Y.; Nabae, A. Instantaneous Reactive Power Compensators Comprising Switching Devices without Energy Storage Components. *IEEE Trans. Ind. Appl.* **1984**, *IA-20*, 625–630. [CrossRef]

22. Suh, Y.; Lipo, T.A. Modeling and analysis of instantaneous active and reactive power for PWM ac/dc converter under generalized unbalanced network. *IEEE Trans. Power Deliv.* **2006**, *21*, 1530–1540. [CrossRef]

23. IEEE Recommended Practices and Requirements for Harmonic Control in Electrical Power Systems. IEEE Std 519-1992. 1993; pp. 1–112. Available online: https://ieeexplore.ieee.org/document/210894 (accessed on 18 October 2021).